Journal of Inorganic and General Chemistry
ZAAC
Zeitschrift für anorganische und allgemeine Chemie
www.zaac.wiley-vch.de
RESEARCH ARTICLE
DOI: 10.1002/zaac.202200213

5-Amino-2-isopropenyltetrazole and its Cupric Chloride Complex: Synthesis, Structure and Magnetism

Sergei V. Voitekhovich,*[a] Alexander S. Lyakhov,[a] Ludmila S. Ivashkevich,[a] Vadim E. Matulis,[a] Yuri V. Grigoriev,[a] Jennifer Klose,[b] Berthold Kersting,[b] and Oleg A. Ivashkevich[a]

A new tetrazole ligand, 5-amino-2-isopropenyltetrazole, was prepared by regioselective alkylation of 5-aminotetrazole with allyl bromide in sulfuric acid followed by dehydrobromination of intermediate 5-amino-2-(1-bromopropan-2-yl)tetrazole. 5-Amino-2-isopropenyltetrazole (L) was found to react with copper(II) chloride to generate complex $[CuL_2Cl_2]_n$. The ligand and its complex were characterized by single crystal X-ray and thermal analyses. Complex $[CuL_2Cl_2]_n$ presents 1D coordination polymer, formed at the expense of double chlorido bridges between neighbouring octahedral coordinated Cu^{II} cations. Tetrazole ligand acts as monodentate ligand coordinated by Cu^{II} cations *via* the heteroring N^4 atoms only. Magnetic studies revealed that the copper(II) ions were weakly antiferromagnetically coupled. Natural bond orbital analysis was performed to explain the structural peculiarities of the ligand. Its basicity and the relative stability of the protonated forms were investigated using MO calculations.

Introduction

5-Aminotetrazole (**1**) and its derivatives are a family of unique nitrogen heterocycles with very high nitrogen content and moderate thermal stability together with large positive enthalpies of formation.[1] Such combination of properties determines the significant interest in them as energetic materials,[1–4] gas-generators and blowing agents.[5,6] Aminotetrazoles are also useful ligands for preparation of coordination compounds, which are attractive as green pyrotechnics,[7] low-toxic primary explosives,[8] catalysts,[9] promising anticancer agents[10] and precursors for preparation of nanoporous metallic materials.[11] Among 5-aminotetrazole derivatives, N^2-substituted ones are least studied as ligands. Only coordination compounds of 5-amino-2-methyltetrazole and 5-amino-2-*tert*-butyltetrazole have been prepared and characterized by X-ray analysis. In particular, silver perchlorate,[12] copper(II) chloride and bromide,[13] copper(II) chlorate,[14] bromate,[15] perchlorate[16] and platinum(II) chloride[17] complexes with 5-amino-2-methyltetrazole have been reported. For 5-amino-2-*tert*-butyltetrazole, only copper(II), platinum(II) and palladium(II) chloride complexes have been characterized.[18]

In continuation of our earlier synthetic, structural and magnetic investigations of cupric complexes with tetrazole ligands,[19,20] here we report new ligand from series of 5-amino-2-R-tetrazoles, having isopropenyl group as substituent R, as well as its cupric chloride complex.

Results and Discussion

Synthesis

For preparation of target 5-amino-2-isopropenyltetrazole (**3**), we applied the procedure previously developed for 5-R-2-isopropenyltetrazoles, where R = H, Me, Ph, CF_3.[21] This procedure is based on acid-catalyzed alkylation. It consists in the interaction of 5-R-tetrazoles with 1-halopropan-2-ols or allyl bromide in 96% sulfuric acid, which leads to the regioselective formation of N^2-(1-halopropan-2-yl)tetrazoles. We found that tetrazole **1** reacts with allyl bromide giving only a single product, identified as 5-amino-2-(1-bromopropan-2-yl)tetrazole (**2**) (Scheme 1).

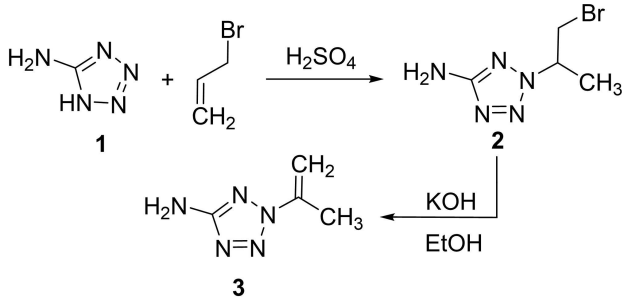

Scheme 1. Synthesis of 5-amino-2-isopropenyltetrazole.

[a] *Dr. S. V. Voitekhovich, Dr. A. S. Lyakhov, Dr. L. S. Ivashkevich, Dr. V. E. Matulis, Y. V. Grigoriev, Prof. Dr. O. A. Ivashkevich*
Research Institute for Physical Chemical Problems of the Belarusian State University
Leningradskaya Street 14, Minsk 220006, Belarus
E-mail: azole@tut.by
[b] *J. Klose, Prof. Dr. B. Kersting*
Institut für Anorganische Chemie, Universität Leipzig,
Johannisallee 29, 04103 Leipzig, Germany

Supporting information for this article is available on the WWW under https://doi.org/10.1002/zaac.202200213

The obtained compound **2** was attributed to 2,5-disubstituted tetrazoles based on ^{13}C NMR chemical shift of the tetrazole ring C^5 atom. The observed value of 166.9 ppm is in accordance with the data on related 5-aminotetrazoles, e.g. 5-amino-2-methyltetrazole (167.2 ppm), whereas corresponding chemical shift for 5-amino-1-methyltetrazole is 155.8 ppm.[22] By analogy with alkylation of other 5-R-tetrazoles,[21] the observed N^2-regioselectivity is caused by the high acidity of the reaction media which leads to the protonation on the tetrazole ring N^4 atom. Further alkylation of symmetrical 5-amino-1H-tetrazol-4-ium cation proceeds on $N^2(N^3)$ atoms only. Subsequent dehydrobromination of **2** was carried out in ethanol using potassium hydroxide, and ligand **3** was isolated in 48% overall yield after two steps. Structure of **3** was confirmed by NMR data and single crystal X-ray analysis.

Complexation of ligand **3** with copper(II) chloride was carried out in 1,2-dichloroethane-ethanol mixture giving light green crystalline complex $[CuL_2Cl_2]_n$ (**4**) in 76% yield. Single crystals suitable for X-ray analysis were picked up directly from the reaction mixture. X-ray powder diffraction data of polycrystalline complex **4** showed its purity (Figure S1).

Synthesized ligand **3** as well as its complex **4** are stable on air under usual conditions and not sensitive to impact and friction. Differential scanning calorimetry and thermogravimetric analysis (TGA) of **3** showed that its decomposition started right after melting, which occurs at 88 °C, and proceeded in one main step with endothermal peak at 187 °C (Figure S2).

Complex **4** decomposes exothermically with maximum heat release at 147 °C (Figure S3). Based on data on thermal decomposition of 5-R-2-isopropenyltetrazoles[23] one can assume formation of molecular nitrogen on initial stage of thermolysis of complex **4**. This is in agreement with TGA data. In particular, on the first stage of thermolysis (140–150 °C) measured weight loss is ~18%. It may correspond to the release of two molecules of nitrogen per CuL_2Cl_2 unit (calculated loss is 14.6%). Observed total weight loss of ~69% may indicate complete destruction and removal of organic ligand, since calculated content of L in CuL_2Cl_2 is 65.1%.

Crystal Structures

The crystal structures of ligand **3** and complex **4** were obtained from single-crystal X-ray analysis. Crystal data of **3** were obtained at 100 K, but complex **4** was investigated at temperatures 100 K and 296 K. Since the complex does not undergo phase transition in the range 100–296 K, its structural data only for 100 K are discussed here. Crystal data, data collection, and structure refinement details for both compounds at 100 K are summarized in Table 1. Table S1 contains such data for complex **4** at room temperature.

Ligand **3** crystallizes in the triclinic space group $P\bar{1}$, with two molecules in the unit cell. The asymmetric unit includes one molecule, shown in Figure 1. All atoms are in general positions. Bond lengths in the tetrazole ring show expected values, ranged from 1.3235(12) Å to 1.3633(13) Å [for all bond lengths, see the caption to Figure 1).

Table 1. Single crystal X-ray data and structure refinement details for ligand **3** and complex **4.**

	3	**4**
Empirical formula	$C_4H_7N_5$	$C_8H_{14}Cl_2CuN_{10}$
Formula weight	125.15	384.73
Temperature (K)	100(2)	100(2)
Crystal system	Triclinic	Monoclinic
Space group	$P\bar{1}$	$P2_1/n$
a (Å)	6.1783(5)	3.81563(5)
b (Å)	7.3793(6)	17.7006(2)
c (Å)	7.4282(6)	10.53289(13)
α (°)	90.3450(10)	90
β (°)	106.3110(10)	98.8200(4)
γ (°)	112.4820(10)	90
V (Å^3)	297.86(4)	702.967(15)
Z	2	2
d_c (g cm^{-3})	1.395	1.818
μ (mm^{-1})	0.100	1.944
Crystal size (mm)	0.35×0.20×0.15	0.38×0.14×0.12
Reflections collected	3054	30811
Independent reflections	1355	2801
R(int)	0.0104	0.0162
Restraints	0	2
Parameters	110	124
Goodness-of-fit on F^2	1.085	1.149
R1/wR2 [I > 2σ(I)]	0.0325/0.0802	0.0187/0.0481
R1/wR2 [all data]	0.0364/0.0825	0.0195/0.0485

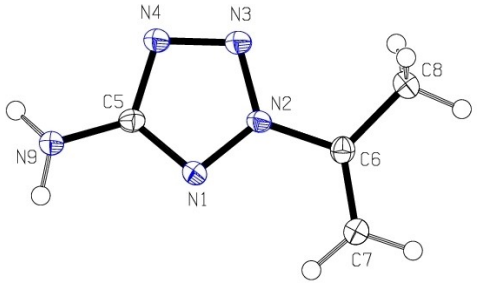

Figure 1. The molecular structure of **3**, showing the atom-numbering scheme. Displacement ellipsoids of non-H atoms are drawn at the 50% probability level, and hydrogen atoms are shown as spheres of arbitrary radii. Bond lengths in the molecule (Å): N1–N2 = 1.3454(12), N1–C5 = 1.3299(13), N2–N3 = 1.3235(12), N3–N4 = 1.3246(12), N4–C5 = 1.3633(13), C5–N9 1.3597(14), N2–C6 1.4336(13), C6–C7 1.3402(15), C6–C8 1.4764(14).

In the molecule of **3**, fragment C5–NH_2 shows close to planar geometry, with the sum of the valence angles around the amino N atom of *ca* 348°. The dihedral angle between the l.s. planes of the tetrazole ring and the amino group is 32.1(9)°, both amino H atoms being located on the same side of the tetrazole ring plane. The flattened geometry of the amino group is favored the conjugation of the N atom lone pair with the tetrazole ring π-system. Despite the closeness to planar geometry, fragment C5–NH_2 is slightly pyramidal.

In the isopropenyl substituent of **3**, single and double bonds are rather different in lengths and show expected values. The dihedral angle between the l.s. planes of the tetrazole ring and

non-hydrogen isopropenyl skeleton is equal to 5.26(5)°. In general, non-hydrogen skeleton of the entire molecule is planar within 0.0452(9) Å. Taking into account the observed position of the isopropenyl double bond relative to the tetrazole ring, the molecule presents *S-cis*-(N^1) conformer.

In the crystal structure of **3**, there are classic intermolecular hydrogen bonds N9–H9A···N3[a] [hydrogen bond geometry: $D\cdots A = 3.2365(13)$ Å, D–H···$A = 166.2(12)°$], and N9–H9B···N4[b] [hydrogen bond geometry: $D\cdots A = 3.0797(13)$ Å, D–H···$A = 171.0(13)°$] between the amino H atoms and the tetrazole ring nitrogen atoms of neighboring molecules. Symmetry codes: (a) $x-1, y, z$; (b) $-x, -y, -z$. These bonds form polymeric chains extending along the *a* axis and containing hydrogen-bonded rings $R^2_2(8)$ and $R^2_2(10)$ (Figure 2). Crystal packing of the compound, shown in Figure 3, demonstrates ribbon-like character of the chains.

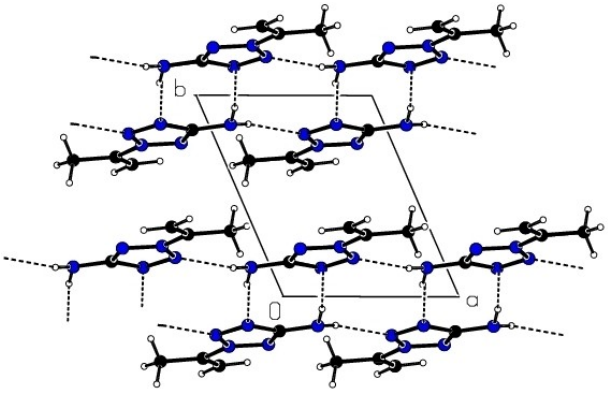

Figure 2. Crystal packing of **3**, viewed along the *c* axis. Dashed lines show hydrogen bonds, forming hydrogen-bonded polymeric chains.

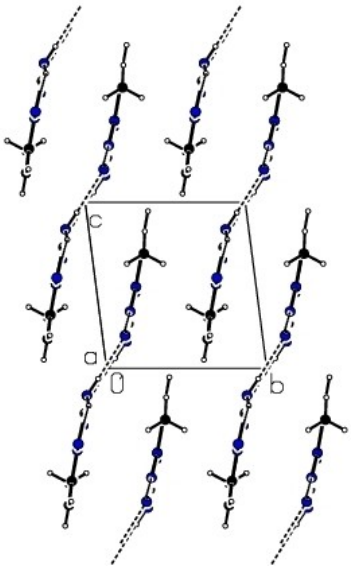

Figure 3. Crystal packing of **3**, viewed along the *a* axis. Dashed lines show hydrogen bonds.

Complex **4** crystallizes in the monoclinic space group $P2_1/n$, with two formula units in the unit cell. The asymmetric unit contains half a Cu^{II} cation, one chloride anion and one ligand molecule (Figure 4). The copper cation lies on inversion center, whereas chloride anion and all ligand atoms are in general positions. The isopropenyl substituent reveals static disorder over two positions, corresponding to *S-trans*-(N^1) and *S-cis*-(N^1) conformers of ligand molecule, with site occupancies 0.588(14) [position A] and 0.412(14) [position B], respectively. It should be noted, that practically the same occupancies were found in this complex at 296 K, namely 0.594(19) [position A] and 0.406(19) [position B].

Complex **4** presents 1D coordination polymer, formed at the expense of double chlorido bridges between neighboring copper cations. In the polymeric chain, running along the *a* axis, neighboring copper cations are separated by 3.8156(1) Å, and the angles Cu–Cl–Cu are of 92.448(6)°.

The Cu1 cation is surrounded by two tetrazole ligands, coordinated *via* the tetrazole ring atoms N4, N4[a], and by four chloride anions Cl1, Cl1[a], Cl1[b], Cl1[c] (symmetry codes as in Table 2). They form considerably distorted octahedral coordination of the metal, with anions Cl1[b] and Cl1[c] in the axial positions of the octahedron. Whereas Cu–N and equatorial Cu–Cl bonds are usual, the axial Cu–Cl bonds are considerably elongated (Table 2), being semi-coordinated or even electrostatic in nature.

In the structure of **4**, the tetrazole ring and the amino group show the dihedral angle between their l.s. planes of 31.3(17)°,

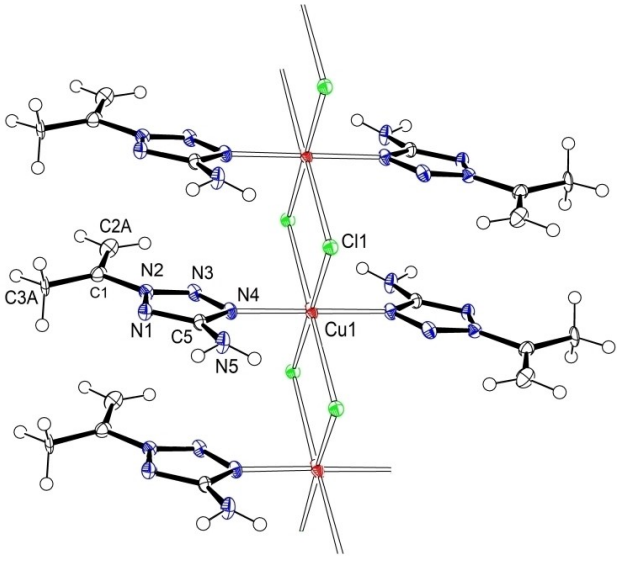

Figure 4. A fragment of the coordination chain in the crystal structure of complex **4**, with the atom numbering for the asymmetric unit. Displacement ellipsoids of non-H atoms are drawn at the 50% probability level, and hydrogen atoms are shown as spheres of arbitrary radii. Disordered isopropenyl substituent is shown in *S-trans*-(N^1) position. Bond lengths in the ligand molecule (Å): N1–C5 1.3374(10), N1–N2 1.3485(10), N2–N3 1.3077(10), N2–C1 1.4361(11), N3–N4 1.3257(10), N4–C5 1.3677(10), N5–C5 1.3492(11), C1–C2 A 1.353(8), C1–C2B 1.333(11), C1–C3 A 1.459(7), C1–C3B 1.459(10).

Table 2. Coordination bond lengths (Å) in the crystal structure of **4**.

Cu1–N4, N4[a]	2.0326(7)
Cu1–Cl1, Cl1[a]	2.27290(18)
Cu1–Cl1[b], Cl1[c]	2.96925(19)

Symmetry codes: (a) 2−*x*, 1−y, 2−*z*; (b) 1+*x*, *y*, *z*; (c) 1−*x*, 1−*y*, 2−z.

being close to that in free ligand [32.1(9)°]. The dihedral angle between l.s. planes of the tetrazole ring and non-hydrogen isopropenyl skeleton is equal to 12.5(3)° for *S-trans*-(N^1) conformer and 4.6(3)° for *S-cis*-(N^1) conformer. The latter value is close to that in free ligand [5.26(5)°], including the same conformer.

In complex **4**, there are classic hydrogen bonds N–H···N of the amino H atoms with the tetrazole ring N atoms of neighboring coordination chain to give hydrogen-bonded layers, parallel to the *ac* plane (Table 3, Figure 5). Hydrogen bonds N–H···Cl, taking place inside the coordination chain, are additional in these layers. Non-classic hydrogen bonds C–H···Cl of H atoms of disordered isopropenyl substituent in position A link neighboring layers into three-dimensional network. Isopropenyl substituent in position B does not participate in hydrogen bonds. This circumstance can be responsible for the fact that site occupancy factor for position A, related to *S-trans*-(N^1) conformation, is greater than that for position B, related to *S-cis*-(N^1) conformation.

Table 3. Hydrogen bond geometry (Å and °) in the crystal structure of **4**.

D–H···A	D–H	H···A	D···A	<(D–H···A)
N5–H5 A···N1[d]	0.858(15)	2.274(15)	3.1287(10)	174.2(14)
N5–H5B···Cl1[b]	0.832(15)	2.434(15)	3.2412(8)	163.9(14)
C2A–H2A2···Cl1[e]	0.95	2.81	3.753(10)	171

Symmetry codes: (b) 1+*x*, *y*, *z*; (d) 2−*x*, 1−*y*, 1−*z*; (e) $^1/_2$−*x*, $^1/_2$+*y*, $^3/_2$−*z*.

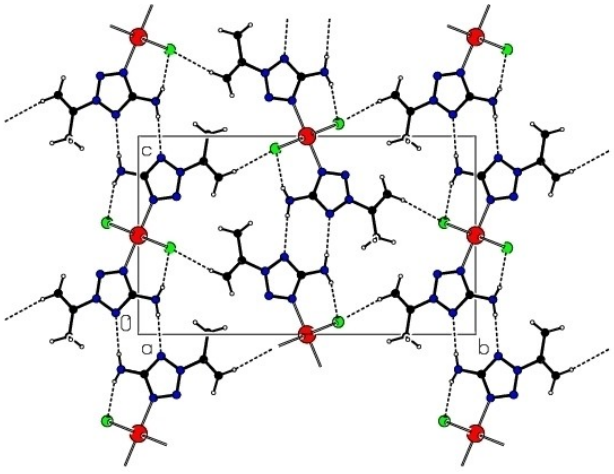

Figure 5. Crystal packing of complex **4**, viewed along the *a* axis. Dashed lines show hydrogen bonds.

Quantum-chemical studies

Calculation of relative energies ΔG^0_{298} of *S-cis*-(N^1) and *S-trans*-(N^1) conformations of 5-amino-2-isopropenyltetrazole molecule showed that *S-cis*-(N^1) conformer is somewhat more stable in comparison with *S-trans*-(N^1) one in both gas-phase (isolated molecule) and polar medium (solution) (Table S2). This result agrees with the obtained X-ray structure of **3**, showing *S-cis*-(N^1) conformation of the molecule.

In order to investigate the influence of medium on structural parameters of 5-amino-2-isopropenyltetrazole, geometry optimization was carried out for the following objects: (a) isolated molecule; (b) molecule in aqueous solution (continuum model), and (c) central molecule in "super molecule", involving a central molecule and three hydrogen bonded neighboring ones. The latter calculations allow to study the influence of specific interactions in crystal on the structural parameters of **3**. The initial geometry of the "super molecule" was taken from X-Ray data. The results of the calculations are given in Table S2. By comparing experimental and calculated bond lengths, it is advantageous to use experimental data corrected for libration. The tetrazole ring bond lengths, calculated for *S-cis*-(N^1) conformer of isolated molecule (B3LYP/6-31G*), are in a good agreement with experimental ones, except for N3=N4 (calculated bond length is 0.017 Å shorter than the experimental one). The use of continuum model (solution) or "super molecule" improves agreement of calculated and observed N3=N4 bond lengths. As to exocyclic bonds, there is essential improvement of C5–N9 bond length by using "super molecule" model, but isopropenyl C6–C8 bond length is the same for all models, being essential longer compared with experimental one. When specific interactions are taken into account, the sum of valence angles at N9 atom becomes closer to 360°, which indicates that this group is becoming less pyramidal but more planar.

NBO analysis was carried out to study the nature of electronic delocalization in molecule **3** and the influence of electronic delocalization on the geometry of C5–NH_2 fragment. We examined the energetic importance of donor-acceptor interactions for all possible interactions between orbitals of C=CH_2 and NH_2 groups with orbitals of the tetrazole ring. As seen from Table S3, there is a strong *n*(N9)-π*(N1=C5) interaction between N9 lone pair (donor) and N1=C5 π* (acceptor) in molecule **3**. Perturbation theory analysis shows strong increase of this interaction for "super molecule" in comparison with the isolated molecule, while other interactions do not differ significantly. Another strong interaction appears between N2 lone pair (donor) and C6=C7 π* (acceptor) and corresponds to π-electron conjugation of isopropenyl group and the tetrazole ring. Other interactions are essentially weaker. The energy of *n*(N9)-π*(N1=C5) interaction, calculated by deleting corresponding element from the NBO Fock matrix, is *ca* 130 kJ mol^{-1} for isolated molecule and 174 kJ mol^{-1} for "super

molecule" (Table S3, values in parenthesis), which agrees with perturbation theory estimations. This considerable increase in n(N9)-π^*(N4=C5) delocalization and shortening of C5–N9 bond in crystal relative to isolated molecule should be attributed mainly to intermolecular hydrogen bonds formation. In crystalline **3**, N–H···N hydrogen bonds lead to elongation of bonds N9–H9A and N9–H9B, to increase in the electron density on N9 atom in comparison with isolated molecule, and to increase in electron donation from the nitrogen lone pair orbital n(N9) to the antibonding acceptor π^*(N1=C5) orbital. The strong n(N9)-π^*(N1=C5) interaction in crystals indicates a strong electron delocalization, which, from the valence bond point of view, can be attributed to a considerable contribution of the Lewis structure with separate charges (Scheme 2).

Delocalization energy, associated with n(N2)-π^*(C6=C7) interaction, is *ca* 70 kJ mol^{-1} for both isolated molecule and "super molecule" (Table S3, values in parenthesis) which is in agreement with perturbation theory estimations. For **3**, the calculated potential energy barrier of rotation S-*cis*-(N^1) → S-*trans*-(N^1) is only *ca* 20 kJ mol^{-1} (Figure S5), which is much lower than the estimated energy of the π-electron conjugation of isopropenyl group and the tetrazole ring. This fact can be explained by steric hindrance in planar structures, and also by stabilization of transition state due to donor-acceptor interactions n(N2)-σ^*(C6=C7) and n(N2)-σ^*(C6–C8) (hyperconjugation).

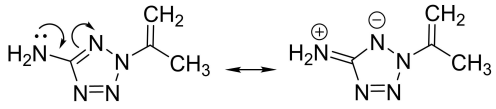

Scheme 2. Possible resonance structures for molecule **3**.

Table 4. Calculated gas-phase basicity *GB* (kJ mol^{-1}) and pK_{BH+} values of **3**.

Protonated atom	*GB*	pK_{BH+}
N1	813.9	−7.59
N3	813.1	−12.75
N4	868.9	−0.76
N9	797.5	−7.63
C7	837.8	−12.75

Calculated molecular electrostatic potentials (MESP) show that local minima are located near the N1, N3, N4 and N9 atoms of molecule **3** (Figure 6b,c). The deepest minimum of MESP is located near N4 atom of the tetrazole ring, while the largest negative NPA charge is predicted on N9 atom of the amino group (Figure 6a). The calculated values of gas-phase basicity and pK_{BH+} show that in gas phase and aqueous solution the atom N4 is the most basic in the molecule **3** (Table 4), which agrees with the calculated MESP distribution. The N9-protonated form is the most unstable in the gas phase. The obtained results agree with experimental and theoretical data for 1,5-diaminotetrazole[24] and 1-vinyl-5-aminotetrazole,[25] showing very low basicity of the amino group nitrogen atom at C5 position of the tetrazole cycle. Calculated pK_{BH+} value of −12.75, corresponding to protonation of molecule **3** on C7 carbon, is in agreement with experimentally obtained values for styrene (−14.1[26]) and isobutylene (−12.5[27]). Electron donor nature of the amino group causes ligand **3** is more basic (pK_{BH+} = −0.76) than unsubstituted tetrazole and 2-methyltetrazole (pK_{BH+} values are −2.68 and −3.25, correspondingly[28]). The obtained results of quantum-chemical calculations are in a good agreement with experimental structural data. Indeed, in complex **4**, tetrazole ligand is coordinated by copper atom *via* the tetrazole ring N4 atom.

Magnetic properties of complex 4

In complex **4**, the presence of chloride bridges, acting as a superexchange pathway between Cu^{II} ions, prompted the present magnetic study. The temperature dependences of magnetic susceptibility (χ) and χT for **4** are shown in Figure 7. Fitting the reciprocal susceptibility (χ^{-1}) data to the Curie-Weiss law in temperature range of 10–300 K (Figure S5) afforded θ = −1.05(4) K, C = 0.459(1) cm^3 mol^{-1} K, and g = 2.21(4). The negative Weiss temperature indicates antiferromagnetic (AFM) coupling between the copper ions. The magnetic susceptibility data were also fitted using a 1D uniform S = $^1/_2$ Heisenberg AFM model.[29,30] The best approximation was obtained by fitting of $\chi(T)$ data. Corresponding theoretical $\chi(T)$ and $\chi T(T)$ plots are shown in Figure 7. The fitted magnetic coupling parameters are J = −0.96(7) cm^{-1} and g = 2.19(5). Value of the exchange interaction constant J indicates very weak magnetic interactions

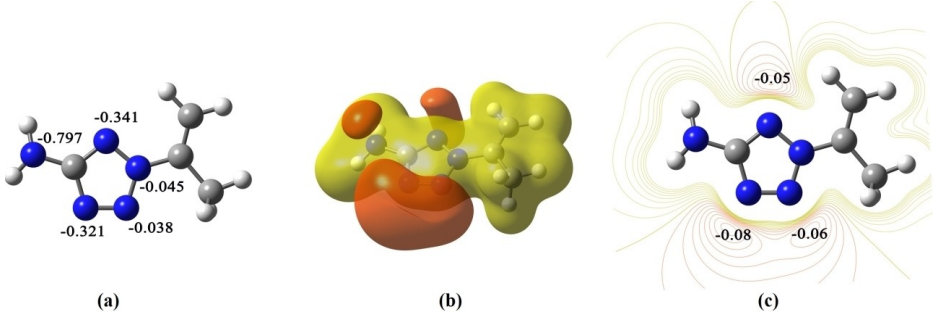

Figure 6. NPA charges (a), MESP surface (b), and MESP contour map (c) for molecule **3**.

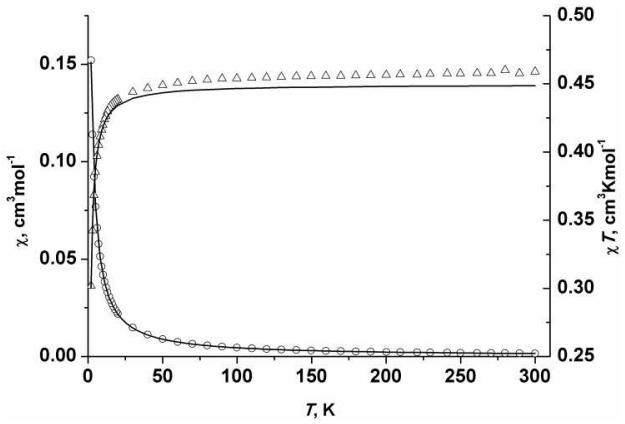

Figure 7. χ *vs T* (o) and χT vs *T* (Δ) functions for complex **4**. The best theoretical fits are illustrated by solid lines.

within the polymeric chain. The weak AFM interaction was also revealed through the magnetization measurements. *M*(*H*) plot measured at 2 K as well as Brillouin plot for isolated $S=^1/_2$ system are presented in Figure S6. Experimental *M*(*H*) plot has linear character up to an external field of 0.7 T. The comparison of the shape of the experimental plot with the Brillouin one shows slower magnetization, which is consistent with AFM interaction.

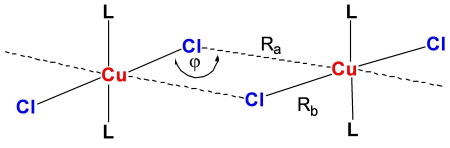

Scheme 3. Fragment of the polymeric chain in complexes $[CuL_2(\mu\text{-}Cl)_2]_n$. The longest and the shortest Cu–Cl bonds are labeled R_a and R_b, respectively.

It is of interest to relate magnetic properties of polymeric chain complexes $[CuL_2(\mu\text{-}Cl)_2]_n$, where L are N-heterocyclic ligands (Scheme 3), to their structural features. Table 5 summarizes magnetic (*J*) and structural parameters of such complexes.[31–42] as well as the present data.

The main parameters that can influence on the *J* value are the length of the longest Cu–Cl bond (R_a) and the angle of Cu–Cl–Cu bridge (φ). In earlier works it was pointed out that the smaller R_a, the stronger magnetic interaction should be expected.[38] But this regularity was observed only for the ligands being very similar in structure. As can be seen from Table 5, the dependence of *J* on φ cannot be approximated by any function. Later, for a number of complexes, the correlation in the form of $J(\varphi/R_a)$ was proposed.[43] However, this correlation is not confirmed by the data, presented in Table 5.

Since the analyzed complexes have coordination chain of the same type and all ligands are coordinated by the metal *via* the heteroring nitrogen atom, one should state that the mentioned above magneto-structural correlations have only limited application. Therefore, more complex combination of structural parameters should be considered to find magneto-structural correlation for these complexes. In the scope of this problem, we should not forget that the nature of the ligand also affects the magnetic characteristics. In particular, in complexes with ligand, containing electron-withdrawing substituents, a weaker magnetic interaction was observed in comparison with electron-donor substituents, which was associated with different electron density on Cu^{II} atoms.[32] In this regard, **4** and $[Cu(ethoxypyrazine)_2Cl_2]_n$[32] have very similar structural parameters, however their *J* values differ significantly. This fact can be explained by lower donor ability of tetrazole **3** compared to ethoxypyrazine, which reduces the electron density at the Cu^{II} atoms in complex **4**. It is clear that the nature of the organic ligand should be taken into account when searching for magneto-structural correlations. Formalization of this contribution is the main way to find an adequate correlation expression.

Table 5. Magnetic and structural parameters of di-chlorido-bridged copper(II) chain complexes $[CuL_2(\mu\text{-}Cl)_2]_n$

L	Cu–Cl bonds lengths R_a (Å)	R_b (Å)	Cu···Cu distances (Å)	φ (°)	J (cm^{-1})	References Structural data	Magnetic data	φ/R_a ($°Å^{-1}$)
pyridine-4-carboxyamide	2.94	2.30	3.72	89.8	−20.8	[31]		30.5
pyrazine-2-carboxyamide	2.86	2.27	3.66	90.3	−18.0	[31]		31.6
methoxypyrazine	2.99	2.28	3.78	90.7	−9.7	[32]		30.3
ethoxypyrazine	2.97	2.29	3.80	91.8	−9.5	[32]		30.9
pyridine	3.03	2.30	3.85	91.5	−9.2	[33]	[34]	30.2
chloropyrazine	2.89	2.28	3.72	91.2	−8.7	[31]		31.6
4-vinylpyridine	3.10	2.38	3.91	90	−8.2	[35]	[34]	29.0
4-methylpyridine	3.19	2.35	3.93	89.1	−7.3	[36]	[37]	27.9
4-ethylpyridine	3.21	2.28	4.00	91.8	−6.8	[38]	[34]	28.6
thiazole	3.00	2.32	3.85	91.9	−3.8	[39]		30.6
2-amino-3,5-dibromopyridine	3.07	2.26	3.92	93.7	−3.4	[40]		30.5
2-amino-3,5-dichloropyridine	2.94	2.27	3.83	93.7	−3.1	[40]		31.9
7-azaindole	3.14	2.28	3.89	90.1	−2.6	[41]		28.7
2-amino-5-nitropyrimidine	2.87	2.25	3.79	94.7	−2.0	[42]		33.0
5-amino-2-isopropenyltetrazole	2.97	2.27	3.82	92.5	−0.96	this work		31.1

Conclusions

We have presented the synthesis, structural and quantum-chemical studies of 5-amino-2-isopropenyltetrazole, which is of interest as new heterocyclic monomer and N-donor ligand. Being coordinated by N^4 endocyclic atom, this ligand generates polymeric chain copper(II) chloride complex, which possesses weak antiferromagnetic coupling between Cu^{2+} cations. Quantum-chemical calculations indicate preference of N4 coordination from the standpoint of the electronic structure of ligand.

Experimental Section

Materials and physical measurements. 5-Aminotetrazole monohydrate and allyl bromide were purchased from Sigma-Aldrich. Copper(II) chloride dihydrate was purchased from Alfa Aesar. Elemental analyses for C, H, and N were performed on a FlashEA 1112 element analyzer. ^{1}H and ^{13}C NMR spectra were recorded on a Bruker AVANCE 500 MHz spectrometer. IR spectra were recorded on a Bruker Vertex 70 spectrometer in diamond cell accessory. The TGA and DSC curves were obtained using a NETZSCH STA449 C thermoanalyzer in a dynamic nitrogen atmosphere (heating rate: 10 °C/min, aluminium oxide, mass 5–6 mg and temperature range from room temperature up to 500 °C). Magnetic properties of complexes were investigated by temperature-dependent magnetic susceptibility measurements in the temperature range between 2 and 300 K in an applied external field of $B = \mu_0 H = 0.5$ T by using a MPMS 7XL SQUID magnetometer. Diamagnetic corrections were applied for the sample holder (gelatine capsule) and the core diamagnetism from the sample (estimated with Pascal's constants).

Synthesis of 5-amino-2-(1-bromopropan-2-yl)tetrazole (2). Allyl bromide (3.19 g, 31 mmol) was added with stirring to 5-aminotetrazole monohydrate (2.58 g, 25 mmol) dissolved in concentrated sulfuric acid (20 mL). The obtained solution was kept at room temperature. After 7 d, the reaction mixture was poured into cold water (100 ml), extracted with dichloromethane (4 x 30 ml). Combined extracts were washed by water (10 ml), aqueous solution of sodium carbonate (5 %, 10 ml), then by water (10 ml) and dried over anhydrous magnesium sulfate. The solvent was evaporated. Obtained oily brown residue was used without purification in next step. ^{1}H NMR (500 MHz, [D$_6$]DMSO): $\delta = 1.54$ (s, 3H, CH_3), 3.75–3.95 (m, 2H, CH_2), 4.96–5.07 (m, 1H, CH) ppm. ^{13}C NMR (126 MHz, [D$_6$]DMSO): $\delta = 166.9$, 59.6, 35.6, 18.6 ppm.

Synthesis of 5-amino-2-isopropenyltetrazole (3). Solution of potassium hydroxide in ethanol (0.5 M, 50 ml) was added dropwise to the solution of crude intermediate **2** in ethanol (50 ml). Reaction mixture was stirred at room temperature for 2 h. Precipitate formed was filtered off. The solvent was evaporated. Obtained solid residue was recrystallized from ethanol-toluene mixture giving colourless crystals of compound **3**. Yield 1.50 g (48 % overall yield after two steps). Mp 88–90 °C. $C_4H_7N_5$ (125.07): C 38.70 (calcd. 38.39); H 5.75 (5.64); N 55.57 (55.97) %. ^{1}H NMR (500 MHz, [D$_6$]DMSO): $\delta = 2.31$ (s, 3H, CH_3), 5.14 (s, 1H, HC=C), 5.61 (s, 1H, HC=C), 6.32 (s, 2H, NH_2) ppm. ^{13}C NMR (126 MHz, [D$_6$]DMSO): $\delta = 166.8$, 138.3, 103.6, 17.6 ppm.

Synthesis of complex 4. Solution of copper(II) chloride dihydrate (0.17 g, 1 mmol) in ethanol (10 ml) was added to the solution of ligand **2** (0.25 g, 2 mmol) in 10 ml of 1,2-dichloroethane-ethanol 1:3 mixture. The reaction mixture was allowed to stand for 6 h at room temperature and thereafter the green crystalline complex **4** was formed. Yield 0.29 g (76 %). $C_8H_{14}Cl_2CuN_{10}$ (384.72): C 24.86 (calc. 24.98); H 3.80 (3.67); N 36.19 (36.41) %. FT-IR (neat): $\tilde{\nu} =$ 3363 s, 3298 s, 3233 s, 3183 s, 3009 s, 2759 m, 1829 w, 1790 w, 1648 s, 1566 s, 1448 s, 1393 m, 1360 m, 1278 m, 1213 m, 1127 w, 1052 w, 1025 m, 1009 m, 911 m, 884 m, 795 w, 748 m, 654 w, 596 w, 423 w cm^{-1}.

X-Ray structure determination. Single crystal X-ray data of free ligand **3** and complex **4** were collected on a SMART Apex II diffractometer using graphite monochromated Mo Kα radiation ($\lambda = 0.71073$ Å). The structures were solved by direct methods (SIR 2014[44]) and refined on F^2 by the full-matrix least squares technique (SHELXL 2014[45]). The intensities were corrected for absorption. For the two compounds, non-hydrogen atoms were refined anisotropically. For ligand **3**, all hydrogen atoms were found from difference Fourier map and refined in isotropic approximation. For complex **4**, only the amino hydrogen atoms were found from difference Fourier map and refined isotropically, but other hydrogens were placed in calculated positions and refined in a "riding" model, with $U_{iso}(H) = 1.5U_{eq}(C)$ for the methyl H atoms and $U_{iso}(H) = 1.2U_{eq}(C)$ for the vinyl H atoms. Molecular graphics was performed with the programs ORTEP-3 for Windows[46] and PLATON.[47] X-ray powder diffraction pattern of polycrystalline **4** was used to control its purity (Figure S1). It was recorded with an EMPYREAN diffractometer (PANalytical, Netherlands) using Cu-$K\alpha$ radiation (Ni-filter) at room temperature.

Crystallographic data for the structures in this paper have been deposited with the Cambridge Crystallographic Data Centre, CCDC, 12 Union Road, Cambridge CB21EZ, UK. Copies of the data can be obtained free of charge on quoting the depository number CCDC-2180133 for ligand **3**, and CCDC-2180134 (296 K) and CCDC-2180135 (100 K) for complex **4.**

MO calculations. MO calculations have been carried out using density functional theory B3LYP method[48] Geometries of all investigated structures were optimized with 6–31G(d) basis set. Natural bond orbital (NBO) analysis was performed using B3LYP/6-311+G(d,p) level. The energies of donor-acceptor interactions were estimated using 2nd-order perturbation theory. Stabilization energy associated with delocalization NBO(i)→NBO(j) was calculated by the Eq. (1).

$$\Delta E_{ij} = q_i \frac{F_{ij}}{\varepsilon_j - \varepsilon_i} \quad (1)$$

where q_i is the donor orbital occupancy; ε_i and ε_j are energies of interacting molecular orbitals, and F_{ij} is the off-diagonal NBO Fock matrix element. The NBO energetic analysis was performed by deleting specified elements from the NBO Fock matrix, diagonalizing this new Fock matrix to obtain a new density matrix, and evaluating total energy (E_{del}). The difference between this "deletion" energy E_{del} and the original energy E provides a useful measure of the energy contribution of the deleted terms. The solvent effects for the pK_{BH+} calculations were evaluated using the polarized continuum model (PCM)[49] with the default parameters for water. The cavity was built up using an united atom (UA) model, i.e. by putting a sphere around each heavy atom. Hydrogen atoms were enclosed in the sphere of the carrier atom. UA model, applied on atomic radii of the UFF force field, has been used. The PCM energies (EPCM) were calculated at the B3LYP/6-311+G(d,p) level using geometries optimized for isolated structures. The solvation Gibbs free energies ($\Delta_{solv}G$) and Gibbs free energies in solution (Gs) were calculated for each species using the Eq. (2) and Eq. (3), correspondingly.

$$\Delta_{solv}G = \mathrm{EPCM} - \mathrm{E} \quad (2)$$

$$Gs = G^0_{298} + \Delta_{solv}G \quad (3)$$

The pK_{BH+} values were calculated using isodesmic reaction method as described previously.[50]

Supporting Information

TG and DSC curves, simulated and experimental XRD powder patterns, data of quantum-chemical calculations, magnetic data.

Acknowledgements

The research was carried out within the framework of the State Program for Scientific Research of the Republic of Belarus "Chemical processes, reagents and technologies, bioregulators and bioorganic chemistry", project 2.1.01.01. Dr. Sergei Voitekhovich acknowledges the support of the research fellowship from the Alexander von Humboldt Foundation (Alumni Program).

Conflict of Interest

The authors declare no conflict of interest.

Data Availability Statement

Research data are not shared.

Keywords: Aminotetrazoles · Copper · Polymeric complexes · DFT · Molecular magnetism

[1] A. I. Lesnikovich, O. A. Ivashkevich, S. V. Levchik, A. I. Balabanovich, P. N. Gaponik, A. A. Kulak, *Thermochim. Acta* **2002**, *388*, 233–251.
[2] N. Fischer, T. M. Klapötke, S. Scheutzow, J. Stierstorfer, *Cent. Eur. J. Energ. Mater.* **2008**, *5*, 3–18.
[3] T. M. Klapötke, C. M. Sabate, A. Penger, M. Rusan, J. M. Welch, *Eur. J. Inorg. Chem.* **2009**, 880–896.
[4] M. Reichel, M. H. Wurzenberger, M. Lommel, M. Kofen, B. Krumm, J. Stierstorfer, T. M. Klapötke, *Z. Anorg. Allg. Chem.* **2012**, *638*, 103–110.
[5] Z. Y. Han, Y. P. Zhang, Z. M. Du, Z. Y. Li, Q. Yao, Y. Z. Yang, *J. Energ. Mater.* **2018**, *36*, 61–68.
[6] C. Cao, D. Zhang, S. Lu, C. Liu, *J. Therm. Anal. Calorim.* **2021**, *143*, 609–618.
[7] G. Steinhauser, T. M. Klapotke, *Angew. Chem. Int. Ed.* **2008**, *47*, 3330–3347; *Angew. Chem.* **2008**, *120*, 3376–3394.
[8] H. Delalu, K. Karaghiosoff, T. M. Klapötke, C. M. Sabate, *Cent. Eur. J. Energ. Mater.* **2010**, *7*, 197–216.
[9] M. Nasrollahzadeh, Z. Nezafat, N. Sadat, S. Bidgoli, N. Shafiei, *J. Mol. Catal.* 2021, **513**, 11788.
[10] M. Nasrollahzadeh, M. Sajjadi, H. Ghafuri, N. Sadat, S. Bidgoli, A. J. L. Pombeiro, S. Hazra, *Coord. Chem. Rev.* **2021**, **446**, 214132.
[11] B. C. Tappan, S. A. Steiner III, E. P. Luther, *Angew. Chem. Int. Ed.* **2010**, *49*, 4544–4565; *Angew. Chem.* **2010**, *122*, 4648–4669.
[12] K. Karaghiosoff, T. M. Klapötke, C. M. Sabate, *Chem. Eur. J.* **2009**, *15*, 1164–1176.
[13] L. S. Ivashkevich, A. S. Lyakhov, A. P. Mosalkova, P. N. Gaponik, O. A. Ivashkevich, *Acta Crystallogr. Sect. C* **2010**, *66*, m114–m117.
[14] M. H. H. Wurzenberger, N. Szimhardt, J. Stierstorfer, *J. Am. Chem. Soc.* **2018**, *140*, 3206–3209.
[15] M. H. H. Wurzenberger, N. Szimhardt, J. Stierstorfer, *Inorg. Chem.* **2018**, *57*, 7940–7949.
[16] J. Stierstorfer, N. Szimhardt, M. H. H. Wurzenberger, T. M. Klapoetke, L. Zeisel, *New J. Chem.* **2019**, *43*, 609–616.
[17] L. S. Ivashkevich, T. V. Serebryanskaya, A. S. Lyakhov, P. N. Gaponik, *Acta Crystallogr. Sect. C* **2011**, *67*, m195–m198.
[18] S. V. Voitekhovich, T. V. Serebryanskaya, A. S. Lyakhov, P. N. Gaponik, O. A. Ivashkevich, *Polyhedron* **2009**, *28*, 3614–3620.
[19] S. V. Voitekhovich, Y. V. Grigoriev, A. S. Lyakhov, L. S. Ivashkevich, J. Klose, B. Kersting, O. A. Ivashkevich, *Polyhedron* **2021**, *194*, 114907.
[20] S. V. Voitekhovich, A. S. Lyakhov, L. S. Ivashkevich, A. N. Lavrov, L. G. Lavrenova, O. A. Ivashkevich, *Z. Anorg. Allg. Chem.* **2021**, *647*, 1633–1638.
[21] S. V. Voitekhovich, P. N. Gaponik, A. O. Koren, *Mendeleev Commun.* **1997**, *7*, 41–42.
[22] W. Bocian, J. Jazwinski, W Kozminski, L. Stefaniak, G. A. Webb, *J. Chem. Soc. Perkin Trans. 2* **1994**, 1327–1332.
[23] S. V. Voitekhovich, P. N. Gaponik, B. G. Kliaus, O. A. Ivashkevich, *Chem. Heterocycl. Compd.* **2002**, *38*, 1422–1423.
[24] V. E. Matulis, A. S. Lyakhov, P. N. Gaponik, S. V. Voitekhovich, O. A. Ivashkevich, *J. Mol. Struct.* **2003**, *649*, 309–314.
[25] A. S. Lyakhov, V. E. Matulis, P. N. Gaponik, S. V. Voitekhovich, O. A. Ivashkevich, *J. Mol. Struct.* **2008**, *876*, 260–267.
[26] J. P. Richard, M. E. Rothenburg, W. P. Jencks, *J. Am. Chem. Soc.* **1984**, *106*, 1361–1372.
[27] R. More O'Ferrall, *Adv. Phys. Org. Chem.* **2010**, *44*, 19–122.
[28] R. E. Trifonov, V. A. Ostrovskii, *Russ. J. Org. Chem.* **2006**, *42*, 1585–1605.
[29] C. P. Landee, M. M. Turnbull, *J. Coord. Chem.* **2014**, 67, 375–439.
[30] D. C. Johnston, R. K. Kremer, M. Troyer, X. Wang, A. Klumper, S. L. Bud'ko, A. K. Panchula, P. C. Canfield, *Phys. Rev. B.* **2000**, *61*, 9558–9606.
[31] N. Hearne, M. M. Turnbull, C. P. Landee, E. M. van der Merwe, M. Rademeyer, *CrystEngComm* **2019**, *21*, 1910–1927.
[32] S. N. Herringer, A. J. Longendyke, M. M. Turnbull, C. P. Landee, J. L. Wikaira, G. B. Jameson, S. G. Telfer, *Dalton Trans.* **2010**, *39*, 2785–2797.
[33] B. Morosin, *Acta Crystallogr. Sect. B* **1975**, *31*, 632–634.
[34] V. H. Crawford, W. E. Hatfield, *Inorg. Chem.* **1977**, *16*, 1336–1341.
[35] M. Laing, E. Horsfield, *Chem. Commun.* **1968**, 735.
[36] M. Laing, G. Carr, *J. Chem. Soc. A.* **1971**, 1141–1144.
[37] W. E. Marsh, E. J. Valente, D. J. Hodgson, *Inorg. Chim. Acta* **1981**, *51*, 49–53.
[38] J. A. C. van Ooijen, J. Reedijk, *Inorg. Chim. Acta* **1977**, *25*, 131–140.
[39] W. E. Estes, D. P. Gavel, W. E. Hatfield, D. J. Hodgson, *Inorg. Chem.* **1978**, *17*, 1415–1421.
[40] K. C. Shortsleeves, L. N. Dawe, C. P. Landee, M. M. Turnbull, *Inorg. Chim. Acta* **2009**, *362*, 1859–1866.
[41] G. A. van Albada, S. Tanase, I. Mutikainen, U. Turpeinen, J. Reedijk, *Inorg. Chim. Acta* **2008**, *361*, 1463–1468.
[42] G. A. van Albada, I. Mutikainen, U. Turpeinen, J. Reedijk, *Inorg. Chim. Acta* **2009**, *362*, 3373–3376.
[43] W. E. Hatfield, *Comments Inorg. Chem.* **1981**, *1*, 105–121.

[44] M. C. Burla, R. Caliandro, B. Carrozzini, G. L. Cascarano, C. Cuocci, C. Giacovazzo, M. Mallamo, A. Mazzone, G. Polidori, *J. Appl. Crystallogr.* **2015**, *48*, 306–309.
[45] G. M. Sheldrick, *Acta Crystallogr. Sect. C* **2015**, *71*, 3–8.
[46] L. J. Farrugia, *J. Appl. Crystallogr.* **1997**, *30*, 565–566.
[47] A. L. Spek, *Acta Crystallogr. Sect. D* **2009**, *65*, 148–155.
[48] A. D. Becke, *J. Chem. Phys.* **1993**, *98*, 5648–5652.
[49] M. T. Cances, B. Mennucci, J. Tomasi, *J. Chem. Phys.* **1997**, *107*, 3032–3041.
[50] S. V. Voitekhovich, Y. V. Grigoriev, A. S. Lyakhov, V. E. Matulis, L. S. Ivashkevich, O. A. Ivashkevich, *Polyhedron* **2019**, *171*, 423–432.

Manuscript received: June 21, 2022
Revised manuscript received: August 31, 2022
Accepted manuscript online: September 1, 2022